Submitted to the Xth International Symposium on Multiparticle Dynamics, Goa, India, Sept. 25-29, 1979

Multiple Correlations and High Transverse Momentum Jets in 147 GeV/c π^-p Interactions

D. Brick, A. M. Shapiro, M. Widgoff

Brown University, Providence, Rhode Island 02912

and

E. D. Alyea, Jr.

Indiana University, Bloomington, Indiana 47401

and

E. S. Hafen, R. I. Hulsizer, V. Kistiakowsky, A. Levy[(a)], P. Lutz[(b)], S. H. Oh,

I. A. Pless, J. P. Silverman, T. B. Stoughton, P. C. Trepagnier, R. K. Yamamoto

Department of Physics and Laboratory for Nuclear Science

Massachusetts Institute of Technology, Cambridge, Massachusetts 02139

and

H. O. Cohn

Oak Ridge National Laboratory, Oak Ridge, Tennessee 37830

and

R. J. Plano, P. Stamer, T. L. Watts

Rutgers University, New Brunswick, New Jersey 08903

and

E. B. Brucker, E. L. Koller

Stevens Institute of Technology, Hoboken, New Jersey 07030

and

W. M. Bugg

University of Tennessee, Knoxville, Tennessee 37916

and

T. Ludlam[(c)], H. D. Taft

Yale University, New Haven, Connecticut 06520

ABSTRACT

We examine multiparticle correlations in a $\pi^- p$ experiment performed by the Proportional Hybrid System Consortium. We used different statistical algorithms by assembling events into groups of particles which are associated by virtue of small relative angles. We found that some of the arising clusters have the properties of high p_T jets. A detailed study of these jet-like clusters is performed.

I. Introduction:

The observed short range rapidity correlations between two particles have been often interpreted in terms of clustering [ref. 1]. But aside from a rather rough comparison with the shape(s) of the correlation(s)--the magnitude of the correlation is fitted by adjusting the cluster size in a cluster model--this interpretation has been without a crucial test. In particular, if the ultimate goal is to be able to tell whether clustering is merely a convenient language, or whether clusters are actually produced, it becomes of interest to try to exhibit clusters from the data of multiparticle events.

On the other hand, the idea of clustering can also be used to describe the properties of high transverse momentum hadronic jets, particularly in parton-model pictures. But, if hadron jets are exhibited in $e^+e^- \rightarrow$ hadrons, experimentalists still need an operational definition of jets in hadron-hadron $\rightarrow$ hadrons. The problem of "trigger bias" is a well known example of how difficult it is to define a jet [ref. 2]. A review of the methods used, up to now, in order to define hadronic jets can be found in ref. [3].

The aim of this paper is to develop methods to found multiparticle correlations using the full dependence on the four kinematical variables of each particle, and to exhibit clusters experimentally. In Section II we will discuss how to define distances between particles inside one event. Section III will describe the algorithms used to aggregate particles into clusters. By applying these algorithms on 147 GeV/c π^-p data, Section IV will show how to check the results of these "clusterizations" with already published results on the same data. Section V will present our results. Finally, in Sections VI and VII, we will emphasize the study of clusters with large transverse momentum and compare our results with other experiments. Our conclusions will be presented in Section VIII.

II. Distances Between Particles in Minkovsky-Space

The object of this study is to assemble each event into groups of particles which are somehow associated in full momentum-space, and not just in a one-dimensional space as in, for instance, the rapidity gap method. We limit ourselves in this paper to methods based on nearest neighbor techniques. Thus, we have to define a distance between two particles of the same event, each particle being regarded as a point in the Minkovsky-space of energy-momentum.

Let us define p_i, $\vec{p}_i$, E_i, m_i respectively the 4-momentum vector, the 3-momentum one, the energy and the mass of particle i. We have actually used three different distances:

(1) $d_1^2 (p_i, p_j) = M_{ij}^2 - (m_i + m_j)^2$

where M_{ij} means effective mass of particles i and j

(2) $d_2 (p_i, p_j) = \mathrm{ch}^{-1} \dfrac{p_i \cdot p_j}{m_i m_j}$

where $p_i \cdot p_j$ is the Lorentz dot-product of the 2 four-vectors

(3) $d_3 (p_i, p_j) = \cos^{-1} \dfrac{\vec{p}_i \cdot \vec{p}_j}{|\vec{p}_i||\vec{p}_j|}$ computed in the center of mass frame

These distances have the following properties:

- They are positive.
- $d_3 = 0$ if $\vec{p}_i$ and $\vec{p}_j$ are parallel and in the same direction.

  d_1 and d_2 are zero only if two conditions are fulfilled at the same time:

  $d_3 = 0$ and $\beta_i = \beta_j$, where $\beta = |\vec{p}|/E$ is the velocity.
- d_2 and d_3 obey the triangle inequality, but not d_1.
- d_1 and d_2 are Lorentz invariants; d_3 depends on the system in which it is computed (we have chosen the center of mass frame).
- d_1 has dimension of a mass, the two others are dimensionless.

The main differences between these distances are:

. d_1 and d_2 are related together by this relation

$$d_2 = ch^{-1}\left(1 + \frac{d_1^2}{2m_i m_j}\right) \qquad (4)$$

Consequently, they differ only because of the presence of the masses in (4). Table 1 gives the value of d_1 and d_2 for different $\pi\pi$ and $p\pi$ masses. For a pion at a same d_1 distance of another pion and a proton, the d_2 distances are different and it is the d_2 distance between that pion and the proton that is the smallest. In other words, metric d_1 has the tendency to find protons at larger distances from pions than metric d_2.

. d_1 and d_2 are analytically related to the effective mass of the two particles, since $2p_i.p_j = M_{ij}^2 - m_i^2 - m_j^2$. Hence, d_1 and d_2 must be large if M_{ij} is large compared to m_i and m_j. On the contrary, d_3 does not depend on the effective mass of the two particles. Appendix I illustrates this point on a simple example.

We will use these three distances, referred to hereafter as, respectively, MAS, KSI and COS distances.

III. Clustering Algorithms

In the rather large panoply of clustering algorithms, we actually have chosen two simple ones, hereafter referred to as MST and CAH.

MST (Minimal Spanning Tree) has been already described by one of us (T.L.) in ref. 4. Let us say that the clusters are defined as the disjoined subtrees of the nearest neighbor graph. It is easily described by saying that:

. Each particle is connected to its nearest neighbor.

. All such connections which are larger than a distance DCUT are broken (this threshold is applied for picking out particles which are clearly isolated in momentum space).

CAH (our acronym for "Classification ascendante hierarchique selon la variance") [ref. 5], can be described as follows:

. Merge into a class the two particles which are the closest to each other, and replace them by their 4-vector sum.

. Recalculate distances between particles or sub-sets (mini-classes) of particles for the partition where the above class had replaced the two particles, using as distance between sub-sets A and B

$$d^2(A,B) = \frac{2n_A n_B}{n_A+n_B}\, d^2(p_A, p_B) \qquad (5)$$

where p_A (p_B) are the 4-momenta of sub-sets A (B)

n_A (n_B) are the numbers of particles inside sub-sets A (B)

. Return to the first step, or stop if that minimum distance is greater than a threshold DCUT.

Formula (5), which weights the distance between sub-sets, has a theoretical root: this chosen criterion is a measure of the increase of inertia involved in the merging, where

$$\text{Inertia (A)} = I(A) = \sum_{i=1}^{n_A} d^2(p_i, p_A)$$

and using the Huyghens theorem:

$$I(AUB) = I(A) + I(B) + \frac{n_A n_B}{n_A+n_B}\, d_2(p_A, p_B)$$

(The factor 2 in (5) is simply to have a weight of 1 when $n_A = n_B = 1$)

Figure 1 describes these two algorithms on a two-dimensional example, with a DCUT = 2.5.

IV. The Philosophy and Choice of the DCUT Thresholds

In MST algorithm, the cut is clearly needed to obtain some one-particle clusters; a part of those have to represent the leading particles that are known to be in the data.

In CAH algorithm, the effect of the cut is different. Of course, as in MST, if two particles are farther than DCUT, they will not be in the same cluster. But even when their distance is originally less than DCUT, they can be in two different clusters, because of the algorithm itself which replaces single particles by subsets of particles. It is the reason why, for a same distance, one has to have

$$\text{DCUT (CAH)} > \text{DCUT (MST)}$$

But DCUT in CAH imposes the size of clusters, which is unlimited in MST.

There is no theoretical best-value for the choice of DCUT, but two simple arguments allow to at least reduce the possible range:

- The $\pi\pi$ mass distribution, computed when the two pions are in the same cluster, has to show a reasonably uncut tail, especially when the cluster is formed only by these two pions. In our data, an empirical lower bound for DCUT is then of the order of 1 GeV for d_1 (MAS), and 4. for d_2 (KSI). No minimum value is required by the d_3 (COS) distance.

- Obviously, the two-prong elastic events have to be two-cluster events. Thus, the higher bound for DCUT is roughly

$$\sqrt{s} \text{ for } d_1 \text{ (MAS)}$$

$$ch^{-1}\left(1 + \frac{s}{2m_a m_b}\right) \text{ for } d_2 \text{ (KSI)}$$

and π for d_3 (COS)

where m_a and m_b are the masses of respectively the beam and the target.

It turns out that the clean diffractive events in the 4-prong 4C fit samples give the same upper limit for DCUT.

Since the possible range for DCUT is large, we have chosen an empirical technique to determine the values of the DCUT. There are certain known "cluster"-type correlations produced when 147 GeV/c pions interact with protons. A general

description of that experiment can be found in ref. 6. We will require that any algorithm and DCUT reproduce these correlations, in particular those published in refs. 7, 8 and 9.

We will denote hereafter in particular choice of algorithm/distance/DCUT but 3 letters as algorithm-code, 3 letters as distance code, and the value of DCUT. As an example

CAHKSI 4.5 means CAH algorithm with d_2 and DCUT = 4.5

With the first one (central fireball cross-section from a rapidity-gap analysis), we can compare the result of the paper with our cross-section of events having 3 or more clusters. This number, considered as a function of DCUT, is obviously a decreasing function. It turns out that MST algorithm is excluded for the use of distances d_1 and d_2, because of a very low value of this number, even for the minimum DCUT - 7mb for MSTKSI 4 and 8mb for MSTMAS 1.0, compared to 13 mb in ref. [7].

Using now ref. [8] (leading particle cross-sections) as comparison, we have to find with our algorithms that these leading particles are actually single particle clusters. Thus, we applied the same cuts in Feynman x as in ref. [8] on our 1-particle clusters and compared the results. It turns out that CAHMAS gives rise to a systematically too high cross-section, especially the proton is too often alone.

At last, using only the events $\pi^- p \to 2\pi^- 2\pi^+ X$, and applying the same cuts as in ref. [9] (off-mass-shell diffraction), we were able to reproduce the results of these three papers for three combinations of algorithm/dist, which are displayed on Table 2.

As a conclusion, the resulting possible value of DCUT is summarized on Table 3. We used only MSTCOS 1.15, CAHKSI 4.7 and CAHCOS 1.75.

V. General Results Obtained by These Clusterization Algorithms

The number of clusters per event is displayed on fig. 2 and the average values are shown on Table 4, as a function of final-state prong number. A few numbers of clusters are created, and the average number of clusters per event increases with multiplicity, by something on the order of .5 clusters per 2 prongs, starting very closely from the value of 2 clusters for the 4-prong events.

The next figure (fig. 3) shows the internal charged multiplicity inside the clusters. On the average, there are slightly less than 3 charged particles per cluster, and the distribution is always narrower than a Poisson's ($\sigma^2 < 2.$).

The mass spectra of multipion groups which emerge when these above-described algorithms are applied to the 147 GeV/c π^-p data are shown in fig. 4, while the charge of the clusters is on fig. 5.

It would be presumptuous to advocate that these clusters should be interpreted as "The Clusters" whose existence is universally inferred in recent literature on multiparticle correlation analysis. However, we would like to emphasize here some indications that those structures indeed reflect real physics...

a) The great stability of the results against any specific algorithm or distance gives us confidence to say that these clusters are not created by the methods, but come from a deeper reason (remember the very different behavior of the two distances!). In particular, the mean mass of the clusters is of the same order for either distance.

b) A crucial point is whether or not the known resonance signals in the data remain intact when events are broken up into groups.

The familiar resonances do not appear as isolated clusters (no ρ^0 signal is seen in the mass spectrum of two-pion groups shown in fig. 4), but are imbedded in larger groups. To very good approximation the Δ^{++} signal remains intact among the clusters, appearing mainly in two-, three-, and four-body groups. This is also

true for the ρ^0 signal, at least for the forward ($Y > 0$) cluster in two-cluster events (fig. 6).

VI. Large Transverse Momentum Clusters

Summarizing the results for the 147 GeV/c data, the correlations in momentum space are such that events exhibit clusters of particles--with typically 3 charged particles per group--having masses and charges similar to those of ordinary particles or resonance states. Whatever dynamics underlie this pattern, it provides a unique and apparently meaningful prescription for reducing multiparticle events to few-body structures. It then becomes of interest to examine the kinematic properties of the clusters.

Figure 7 shows the invariant cross section for the clusters as a function of the transverse momentum of these clusters. The three algorithms/distance combinations show the same behavior, which is just the behavior expected for what are now called high p_T jets, which is shown also in fig. 7 both by a result from a calorimeter experiment [ref. 10] and by the theoretical prediction of ref. [11].

In order to determine if our high p_T clusters are really high p_T jets, we performed two kinds of Monte Carlo analyses.

a) Generating events with the experimental single particle p_T distribution, but no correlation between the outgoing particles, and applying the clustering algorithms on these events, it turns out that the general features (multiplicity, mass and charge) of the found clusters can be matched and actually are matched by fake events, but absolutely not the kinematical properties, especially the p_T distribution superimposed on fig. 7.

b) Generating jets by the Feynman-Field's Monte Carlo program described in ref. [12], with the same internal properties as those found for our high p_T clusters (charged multiplicity and energy), we have checked the efficiency of the

clustering algorithms to detect jets.[1] This efficiency can be measured by the quantity

$$\epsilon = \frac{\text{number of jets found by the algorithm}}{\text{number of generated jets}}$$

and has been found of the order of 75% for every algorithm (Table 5) and more than 60% for jets found by the three algorithms altogether. Figure 8 shows this efficiency as a function of the charged multiplicity inside the generated jet.

If we allow one jet to be not exactly found, by adding also clusters where the missing particles have all a z[2] less than .14, these two percentages respectively rise to nearly 90% and 80%. The losses mainly come from neutral particles, which have been generated by the F. F. program but removed before clustering, in order to be in the same situation as in our experiment.

These two complementary Monte Carlo studies allow us to claim that the used clusterization algorithms are able to exhibit multiparticle correlations, especially those correlations which give rise to high transverse momentum jets. We will now study the properties of these jet-like clusters.

VII. Study of High Transverse Momentum Clusters

From now on, we will call "jet" any cluster with a p_T greater than 1.5 GeV/c. We define a four-momentum for a jet as the sum of the four-momenta of the (charged) particles belonging to that jet.

a) General features: a comparison on an event by event basis, between the different used algorithms, shows a remarkable stability in finding jets. Table 6 clearly demonstrates that if only one-third of the events have exactly the same

---

(1) This program does not generate events, but single jets. We proceeded each jet through any of the three algorithms, as if it were a complete event.

(2) z is the fractional longitudinal momentum of a jet-particle. See par. VII c) for the definition.

clustering in two different algorithms, and only half the clusters are the same, more than 70% of the events having ajet in the first algorithm have also a jet in the second one, and then more than 90% of these jets are similar (identical or differing only by one slow particle).

This stability, which is a further evidence for the existence of jets in our experiment, allows us to study the results of only one clusterization algorithm. For this jet study, we have chosen to keep only CAHKSI 4.7.

Table 6 displays the general characteristics of jet events. This table can be summarized in four points:

. The inclusive cross-section for $\pi^- p \rightarrow$ jet + X is, at our energy, of the order of 10% of the total $\pi^- p$ cross-section.

. Only 10% of jet-events have more than one high p_T jet.

. The probability for finding a jet in one event increases with the internal multiplicity of that event.

. The mean number of clusters found in jet events is slightly higher (3.56) than in all events (2.87).

Turning to the distribution in θ^*, polar angle (in the center-of-mass system) of the jet-axis, shown in fig. 9, it is interesting to note that this is the first analysis showing high p_T jets in the backward hemisphere from a π beam experiment. Two important results arise:

. More jets are produced in the forward hemisphere than in the backward direction.

. The mean charge of these jets seems to be practically linear in θ^*, of the form $< \theta > = -1 + \frac{2\theta^*}{\pi}$.

These two results can easily be explained from the quark content and quark distributions inside the π^-.

b) Momentum balance in jet events.

It is difficult to study the momentum balance in our experiment, since we have no neutral information. Nevertheless, some results can be reached.

1) Planarity:

- Defining the "aplanarity" coefficient as the normalized third eigen value $-\lambda_3-$ of the inertia tensor $\sum_{i=1}^{n} p_{ij}^{\alpha} p_i^{\beta}$, it turns out that the mean value $<\lambda_3>$ of this aplanarity is small for jet-events ($<\lambda_3>^{jet} = .027$) but significantly greater than for all events ($<\lambda_3>^{all} = .015$).

- A more conventional manner to study the planarity is to define a "trigger plane", which is obviously here the plane defined by the beam axis and the jet-axis (in the case of two jet-events, the highest p_T jet-axis), and to study the component out of that plane, p_{out}, the distribution of which is shown on fig. 10. We obtain a mean value

$$<p_{out}> = (.490 \pm .025)\ GeV/c$$

in very good agreement with other experiments [refs. 13, 14, 15], despite the fact that their "trigger plane" does not use a jet axis but the trigger particle axis only.

2) Balance of the p_T of the jet:

For each cluster in our jet-events, let us name p_{in} the p_T component in the "trigger" plane. The mean values $< p_L >$ and $<p_{in}>$ for each cluster are shown in fig. 11 for jet-events which verify $14 < E_{tot} < 20$ ($\sqrt{s} = 16.5$ in our experiment). It is easily seen that if the longitudinal component is well balanced, the p_{in} component is not, despite the fact that the so-called spectator jets (beam and target jets) try to balance that component.

c) Internal properties of these jets.

. The charged multiplicity distribution of jets defined by CAHKSI 4.7 method is shown in fig. 12a. The mean charged multiplicity is $<k> = 3.18$ (some how higher

than the value of 2.74 obtained for all clusters) and the distribution is narrower than a Poisson ($\sigma^2 = 2.38$).

. Figure 12b shows the relative rapidity $\Delta y = |y - y^{jet}|$ of particles inside and outside jets. The very sharp spike at $\Delta y = 0$ for particles belonging to the jet illustrate the well-known correlation in rapidity between particles inside a jet (this correlation has been the first evidence for jets in hadron-hadron collisions), and the flatness of the distribution near $\Delta y=0$ for particles outside the jet can be interpreted as the fact that our algorithms seem to neither lose particles from the jet nor add background particles to the jet.

. To investigate whether the jets are dominated by resonance production at large p_T, fig. 12c shows the two particle mass distribution of jet particles for neutral pairs, treating each particle as a pion. The ρ resonance is seen as a shoulder on an important combinatorial background.

. Finally, it is of interest to study the momentum components of jet particles along the jet axis and perpendicular to it. In fig. 13 is shown the observed distribution of the fractional longitudinal momenta of jet-particles, $z = \vec{p} \cdot \vec{p}_{jet} / |p_{jet}|^2$, compared to other experiments. The low values at $z < 0.1$ are probably due to experimental or methodological loss of low momentum particles, and the rest of the distribution is well compared with the fragmentation of jets produced either by lepton processes or in hadron-hadron collisions.

The distribution of the transverse momentum component q_T of jet particles perpendicular to the jet axis is shown in fig. 14. The exponential distribution has a mean value $\langle q_T \rangle = .280$ GeV/c, not so far from the value observed in e^+e^- annihilation (.350 GeV/c for $E_{CM} \sim 5$ GeV) but considerably smaller than observed in other hadron-hadron experiments ($\sim .50$ GeV/c, see ref. [16]).

VIII. Conclusions

Using a purely statistical algorithm to exhibit multiparticle correlations in a $\pi^- p$ experiment performed in a hybridized bubble chamber at 147 GeV/c, it turns out that some of the arising clusters have the properties of high p_T jets. The observed structure is consistent with the assumption that large-p_T objects originate from scattered hadronic constituents. The study of the momentum balance confirms that these hadronic constituents have to have rather large transverse motion. This first "no bias" jet-experiment shows a strong correlation between the charge of the jet and the production angle of this jet, which is an evidence that the scattering constituents are quarks. This kind of analysis, nevertheless, has to be extended for

- complete (charged + neutral) particle identification.
- better statistics.
- higher energies.
- other beam particles.

This work was supported in part by the U. S. Department of Energy and the National Science Foundation. We gratefully acknowledge the efforts of the 30-inch bubble chamber crew and the scanning and measuring personnel at the participating institutions.

Footnotes and References

a) On leave of absence from Tel-Aviv University, Tel-Aviv, Israel.

b) On leave of absence from Lab. de Physique Corpusculaire, Collège de France, Paris, France.

c) Present address: Brookhaven National Laboratory, Upton, Long Island, New York.

[1] See for example.
R. Diebold, Proceedings of 19th International Conference on High Energy Physics, Tokyo, 1978, and references therein.

[2] M. Jacob and P. V. Landshoff, N. P. B13, 395 (1976).

[3] S. Nielsen, Ph.D. Thesis, Copenhagen, August 1978 (Niels Bohr Institute) unpublished.

[4] T. Ludlam, Yale Report No. C00-3075-210 (March 1978).

[5] J. P. Benzecri et al., "'algorithme de Classification Ascendante Hierarchique. Internal report (unpublished) of the Laboratoire de Statistique Mathematique, Université P. &M. Curie, Paris (1975).
The first idea of such an algorithm applied in high energy physics can be found in: T. Ludlam and R. Slansky, P.R. D16, 100 (1977).

[6] D. Fong et al., N.P. B102, 386 (1976).

[7] I. A. Pless et al., Inclusive and Semi-Inclusive Charge Structure in π^-p Multiparticle Production at 147 GeV/c, contribution to Tokyo Conference (1978) (unpublished).

[8] D. Fong et al., P.L. 53B, 290 (1974).

[9] F. Barreiro et al., submitted to P.R.L.

[10] C. Bromberg et al., Comparison of Hadron Jets Produced by π^- and p Beams on Hydrogen and Aluminium Targets (Fermilab preprint 7000.260).

[11] R. P. Feynman, R. D. Field and G. C. Fox, N.P. B128, 1 (1977).

[12] R. D. Field and R. P. Feynman, N.P. B136, 1 (1978).

We take this opportunity to thank Professor Field for the permission to use his program.

[13] M. Della Negra et al., N.P. B127, 1 (1977).

$\langle P_{out} \rangle = (.53 \pm .02)$ GeV/c (CCHK).

[14] Ref. 2. $\langle p_{out} \rangle = (.501 \pm .004)$ GeV/c (BFS).

[15] Ref. 10. $\langle p_{out} \rangle = (.48 \pm .01)$ GeV/c (E260).

[16] R. Sosnowski, Rapporteur's talk at Tokyo Conference (1978).

Appendix 1

Comparison Between Distances d_2 (KSI) and d_3 (COS)

Let us take three pions, the first one with $p_1 = 10m_\pi$ and the two others with $p_2 = p_3 = m_\pi$, symmetric (angle α) with respect to the first one.

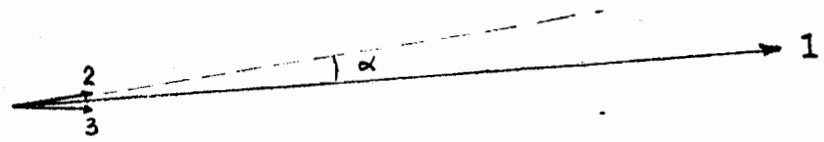

It is easy to compute the different distances between these particles and it turns out that, anyhow α's value is:

$$d_2\ (1,2) > d_2\ (2,3)$$

and $$d_3\ (1,2) < d_3\ (2,3) \qquad \text{(trivial)}$$

Consequently, the two distances are very different.

$M_{\pi\pi}$ (GeV/c^2)	d_1 (MAS)	d_2 (KSI)	$M_{p\pi}$ (GeV/c^2)	d_1 (MAS)	d_2 (KSI)
.3	.110	.768	1.1	.220	.598
.4	.286	1.800	1.2	.527	1.352
.5	.415	2.374	1.3	.727	1.769
.6	.531	2.798	1.4	.893	2.076
.7	.642	3.140	1.5	1.043	2.324
.8	.750	3.428	1.6	1.182	2.534
1.0	.960	3.898	1.8	1.442	2.880
1.3	1.270	4.440	2.0	1.685	3.163
1.6	1.575	4.863	2.5	2.256	3.709

Table 1: Distances (d_1 and d_2) corresponding to given $\pi\pi$ and $p\pi$ effective masses

	published papers	MSTCOS 1.0 (57^0)	MSTCOS 1.2 (69^0)	CAHKSI 4.5	CAHKSI 4.7	CAHCOS 1.5 (86^0)	CAHCOS 1.8 (103^0)
Ref. 7 $\sigma_{NCL\geq 3}$(mb) (central fireball)	$12.9 \pm .8$(sys) $\pm .2$(stat)	13.6	11.2	13.0	11.9	13.9	12.2
Ref. 8 Leading part. (mb)							
P	$.93 \pm .12$	1.11	1.05	.95	.93	.99	.94
N = 4 π^-	$.91 \pm .16$	.83	.79	1.08	1.05	.76	.69
Sum	$1.84 \pm .20$	1.95	1.84	2.03	1.98	1.75	1.63
P	$.40 \pm .13$	.62	.52	.41	.38	.45	.38
N = 6 π^-	$.18 \pm .09$	.25	.22	.44	.41	.19	.16
Sum	$.58 \pm .16$	.87	.74	.85	.79	.64	.54
Ref. 9 $2\pi^+ 2\pi^-$ evts.							
# evts. (x_π -< .93)	633	630	630	630	630	630	630
# evts. NCL = 2 3 part./1 part.		267	312	284	300	279	317
# evts. "A" region	275	246	273	279	290	254	277
Percentage of off mass shell diffraction	$(43.4 \pm 2.6)\%$	39.1%	43.3%	44.3%	46.0%	40.3%	44.0%

Table 2: The choice of DCUT, using references 7, 8, 9 results

("A" region means $M_{3\pi} \leq 2.0$ Gev/c^2)

Algorithm/distance	$DCUT_{min}$	$DCUT_{high}$	Used value
MST MAS	no fit at all		excluded
MST KSI	only ref. 8 can fit		excluded
MST COS	1.10 (63^0)	1.15 (66^0)	1.15 (66^0)
CAH MAS	ref. 8 cannot fit		excluded
CAH KSI	4.5	4.7	4.7
CAH COS	1.55 (89^0)	1.8 (103^0)	1.75 (100^0)

Table 3: Allowed values of DCUT for each algorithm/ distance combination

Topology (number of charged part.)	CAHKSI 4.7	CAHCOS 1.75	MSTCOS 1.15
4	2.09	2.03	2.18
6	2.46	2.52	2.58
8	2.88	3.10	2.92
10	3.38	3.64	3.35
12	3.73	4.19	3.71
14	4.20	4.77	4.42
16	4.52	5.48	4.84
Inclusive	2.87	3.07	2.95

Table 4: Average number of clusters per event

$\epsilon = \frac{\text{jets found in . . .}}{\text{generated jets}}$	Exactly found	All particles missing have $z < .14$
CAHKSI 4.7	.765	.876
CAHCOS1.75	.727	.893
MSTCOS1.15	.753	.881
all three algorithms	.632	.795

Table 5: Efficacity of the clustering algorithms to find jets generated by Field's program

Comparison between	A (%)	B (%)	C (%)	D (%)
CAHKSI 4.7 & MSTCOS 1.15	34.	48.3	71.0	
CAHKSI 4.7 & CAHCOS 1.75	34.	49.2	76.6	91.7
MSTCOS 1.15 & CAHCOS 1.75	55.	62.1	77.3	85.6

A: number of events with exactly the same clustering in the two algorithms.

B: number of clusters found identical in the two algorithms.

C: Number of events having a jet in the two algorithms.

D: among class C, number of jets which are either identical, or varying by only one slow particle (slow means $p < .3$ GeV/c).

Table 6: Comparison between algorithms and distances on an event by event basis

jet = cluster with $p_T > 1.5$ GeV/c

$\sigma_{Tot}(\pi^- p \rightarrow \text{jet} + x)$	$(2.56 \pm .60)$ mb
$\langle p_T \rangle_{jet}$	1.78 GeV/c $(\langle x_T \rangle = .215)$
Total number of jet-events	447 (9% of all events)
Number of events with one jet	402
Number of events with more than one jet	45

Topology of (n_{ch}) event	4	6	8	10	12	14	16
jet/event (%)	2.2	4.8	11.1	18.1	21.8	33.7	36.0

total number of clusters per event (NCL)	2	3	4	≥ 5	
number of jet events	43	232	128	41	

Table 7: General jet characteristics in $\pi^- p \rightarrow$ jet + x at 147 GeV/c

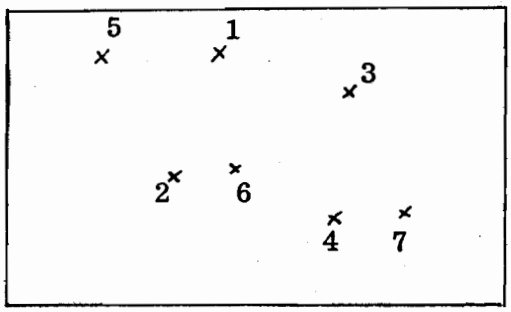

a) a two-dimensional event.

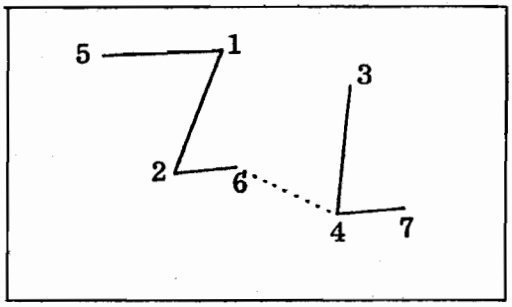

b) The minimal spanning tree of that event: (the link between points 6 and 4 has been broken because no one of these two is the nearest neighbor of the other.) As long as DCUT is greater than 1.7 (the length of the longest link) the MST algorithm gives two clusters (1-2-5-6 and 3-4-7).

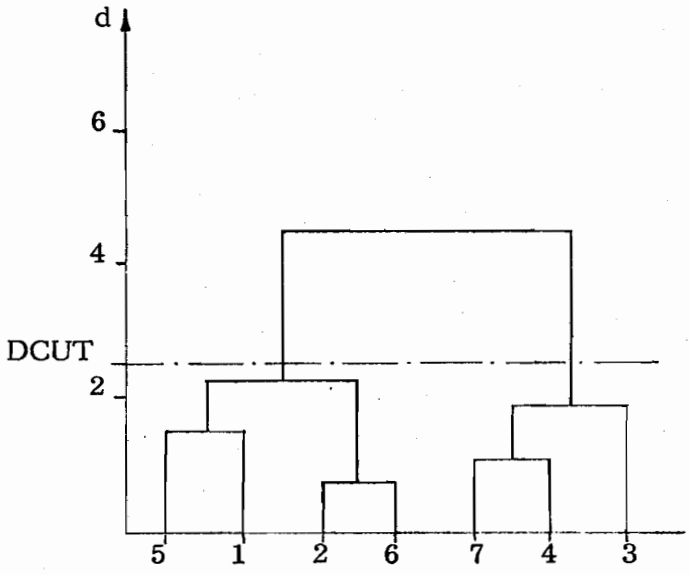

c) CAH algorithm on the same event, with in abscissa the labels of the points and in ordinate the distance at which points or subsets are merged. For a DCUT between 2.2 and 4.5, two clusters (identical to the ones of MST) are obtained.

Figure 1: Principle of the classification algorithms

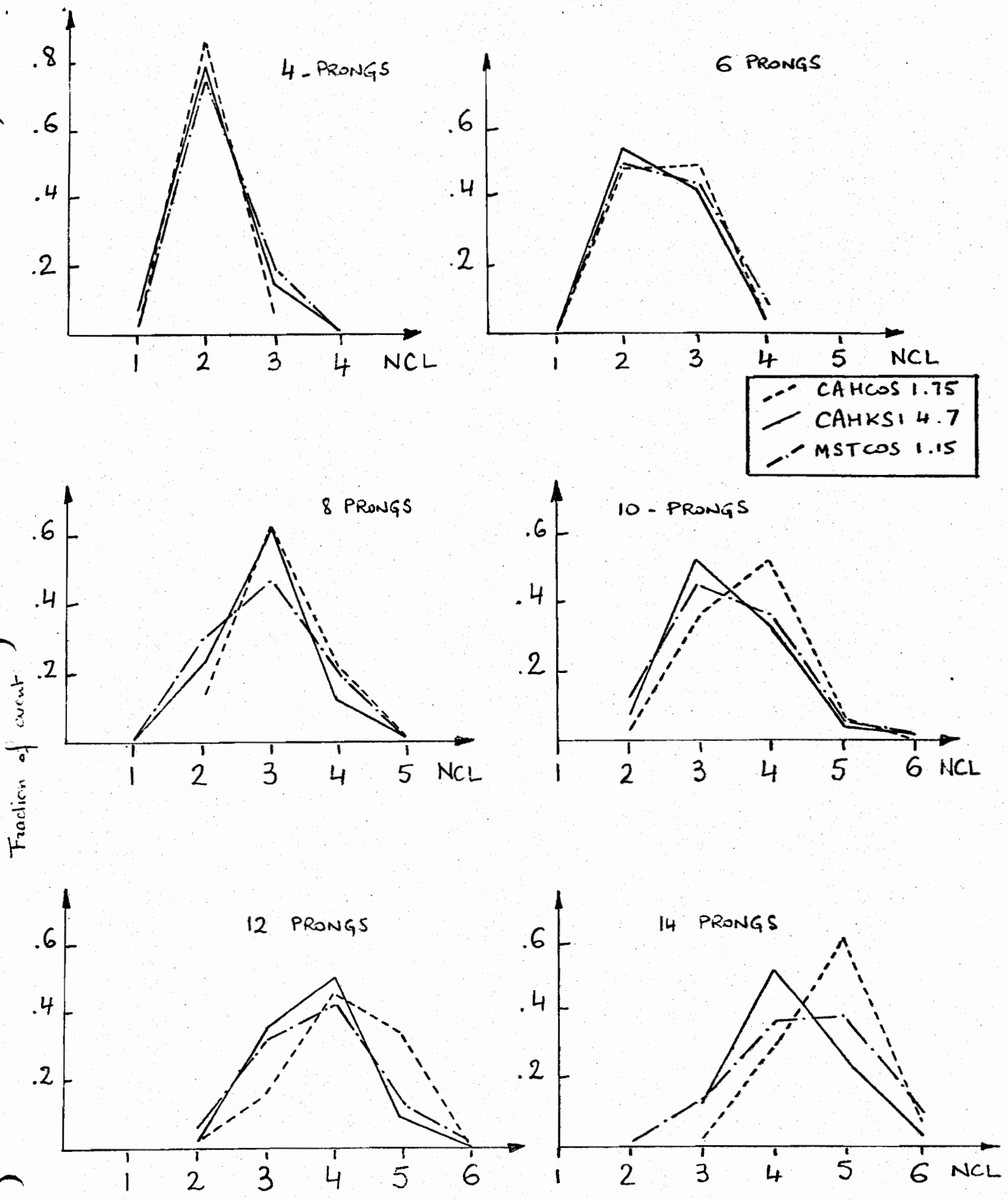

Fig 2. Distribution of the number of clusters (NCL) per event as a function of final state prong number.

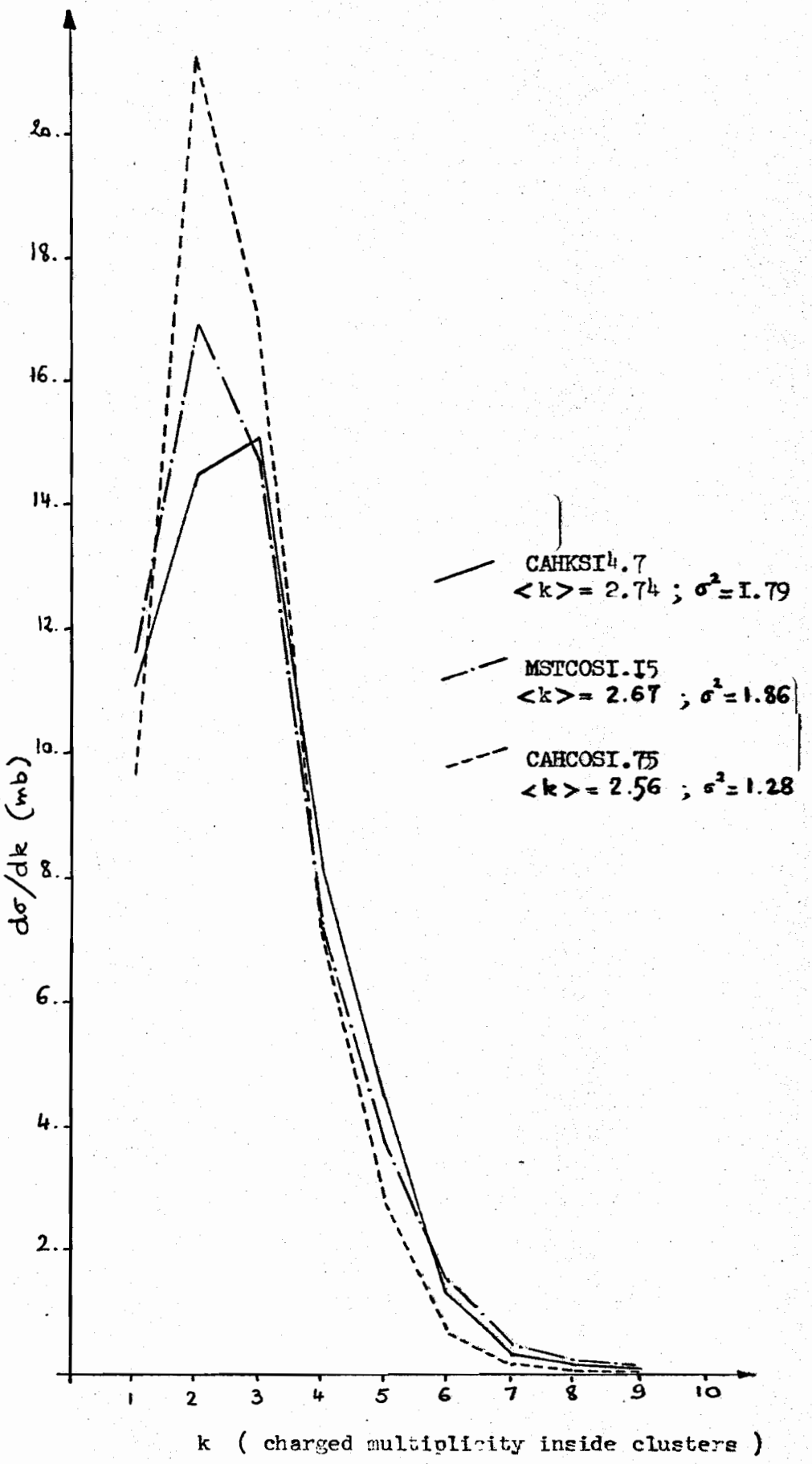
dσ/dk (mb)
20.
18.
16.
14.
12.
10.
8.
6.
4.
2.
1
2
3
4
5
6
7
8
9
10
k (charged multiplicity inside clusters)
CAHKSI4.7
<k>= 2.74 ; σ²= I.79
MSTCOSI.I5
<k>= 2.67 ; σ²= 1.86
CAHCOSI.75
<k>= 2.56 ; σ²= 1.28

Fig. 3

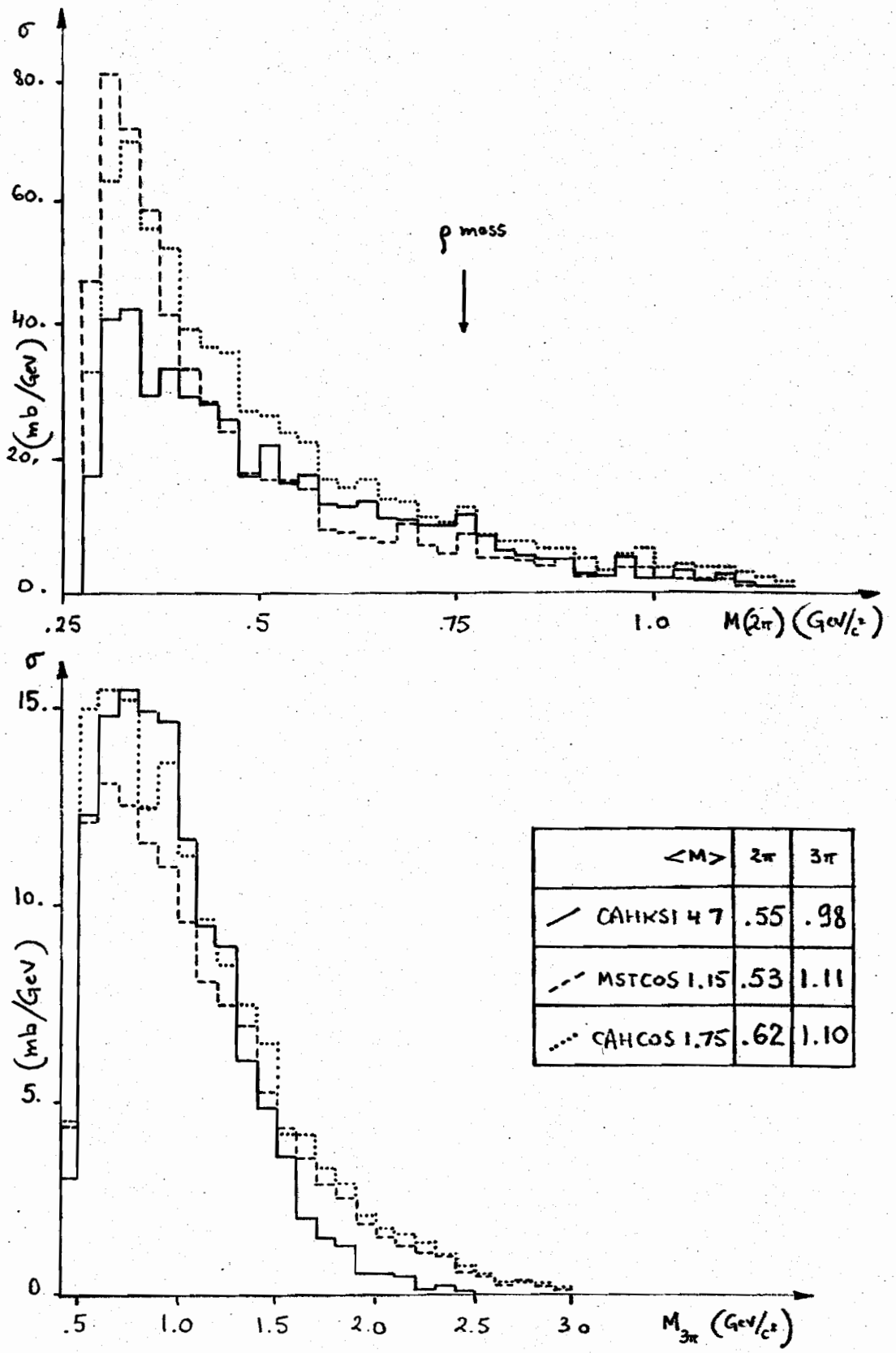

Fig 4: Mass spectra of the (2π) and (3π) groups.

CAHKSI#.7
147 GeV/c π^-p

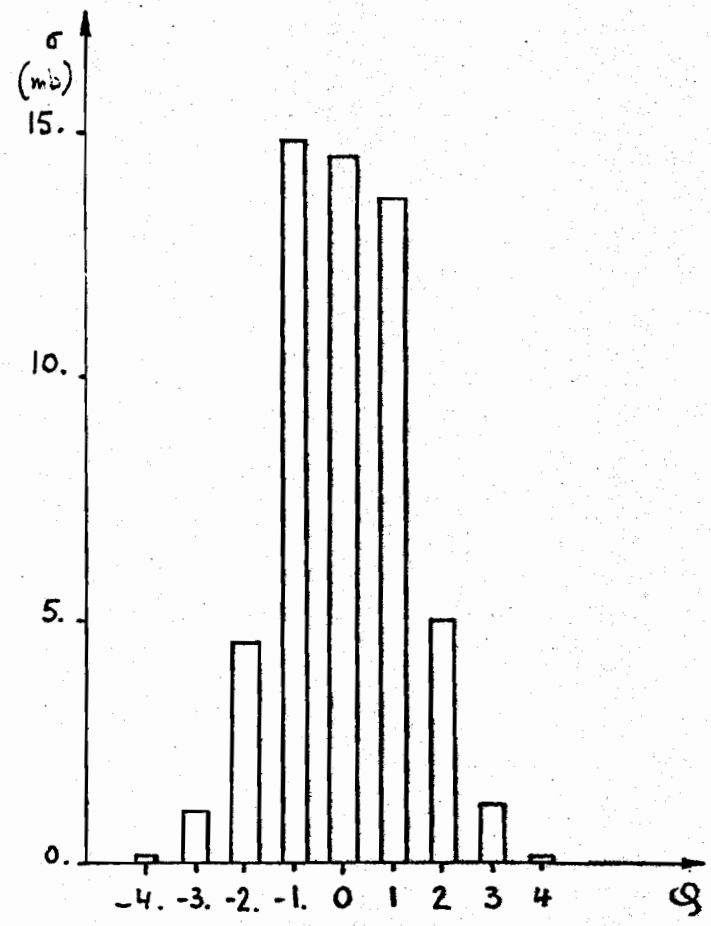

Fig 5 : Charge of clusters

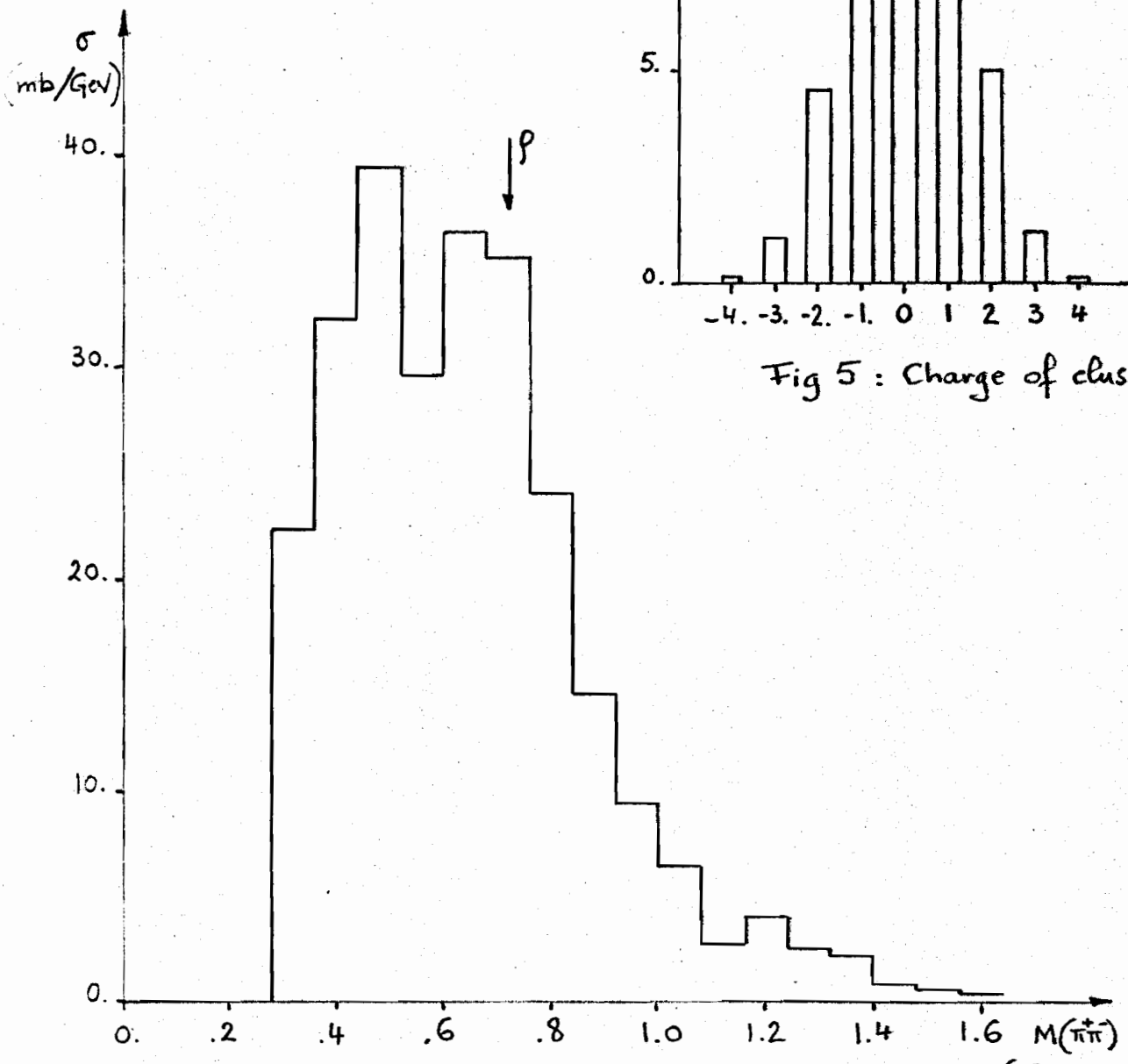

Fig 6 : Effective mass $\pi^+\pi^-$ inside leading forward cluster
(two-clusters events only)

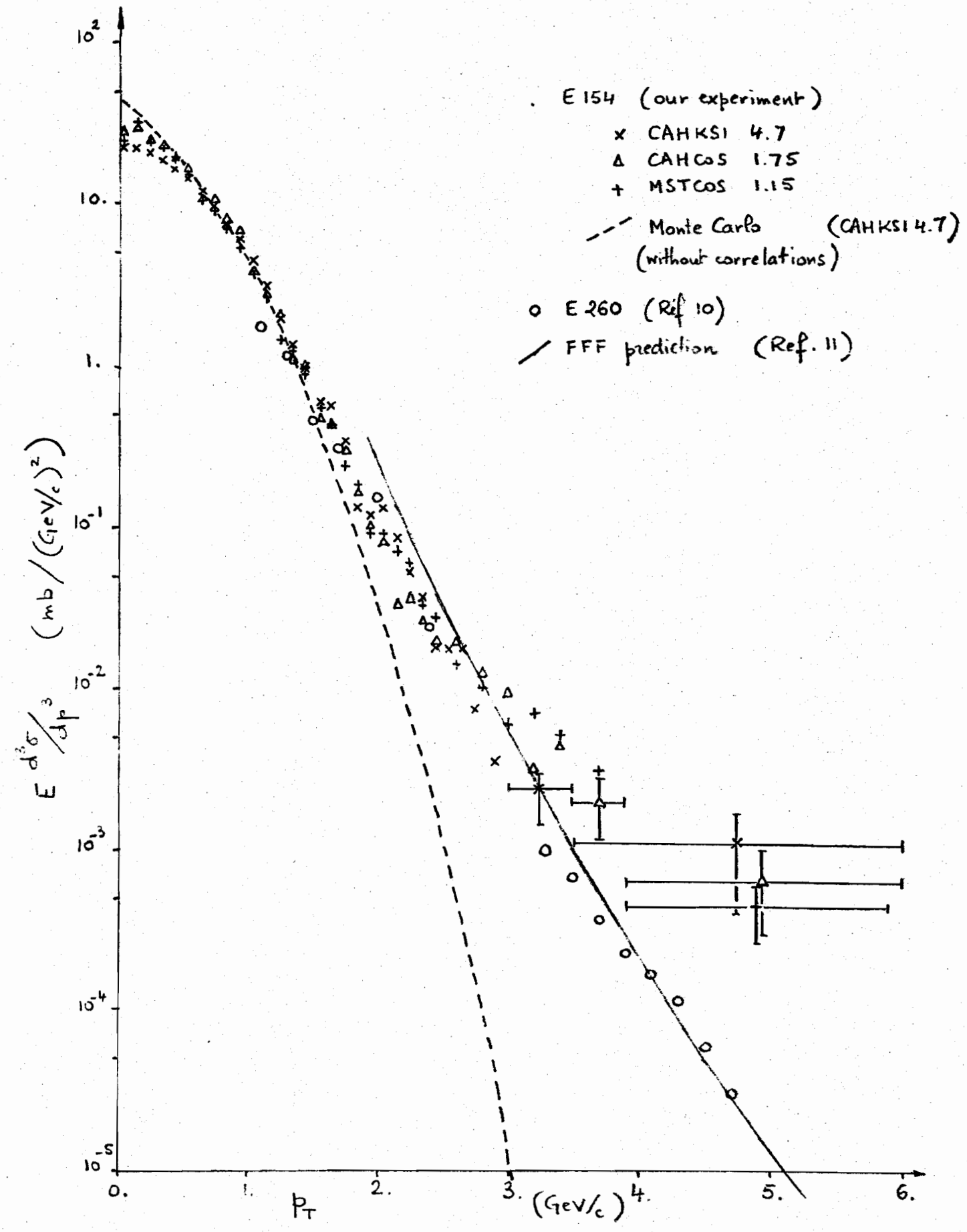

Fig 7 : Invariant cross-section of clusters

$$\varepsilon = \frac{\text{jets found by the algorithm}}{\text{generated jets}}$$

n = charged multiplicity inside generated jet

——— jets exactly found

- - - jets nearly found (missing particles have $z < .14$)

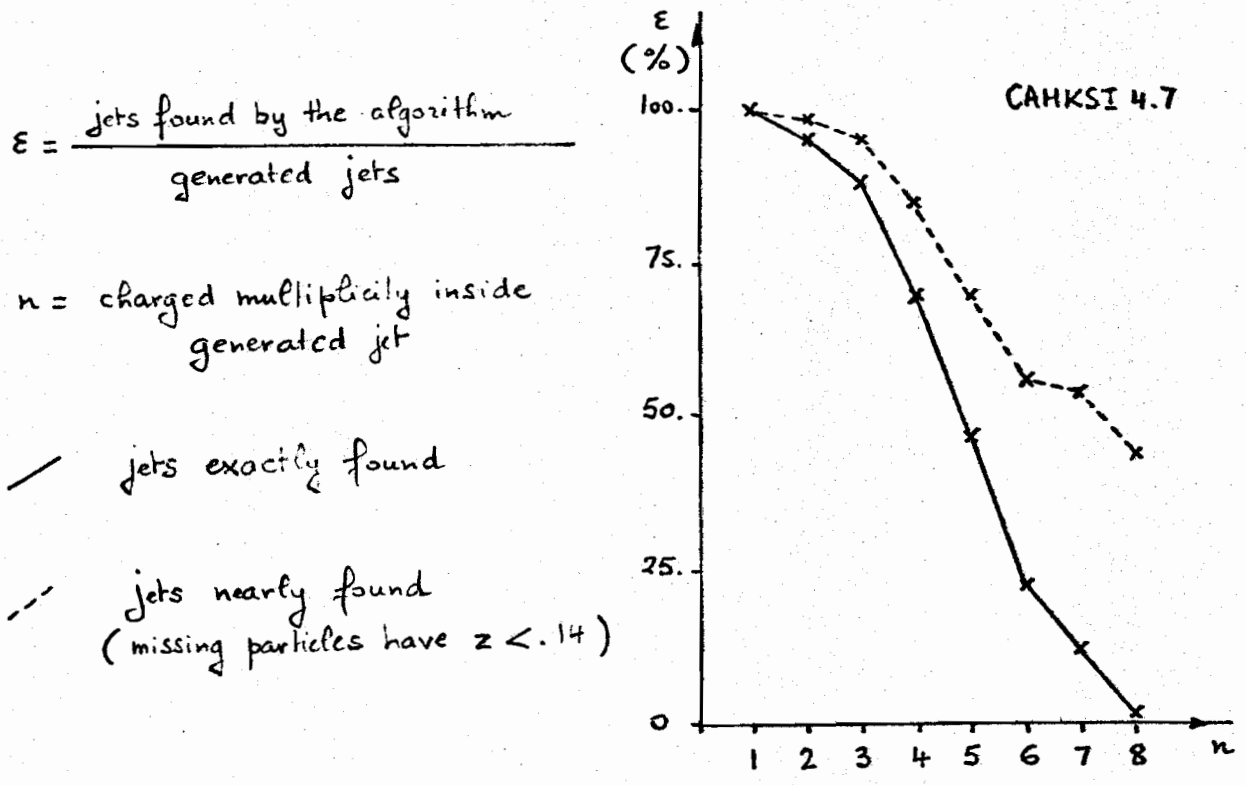

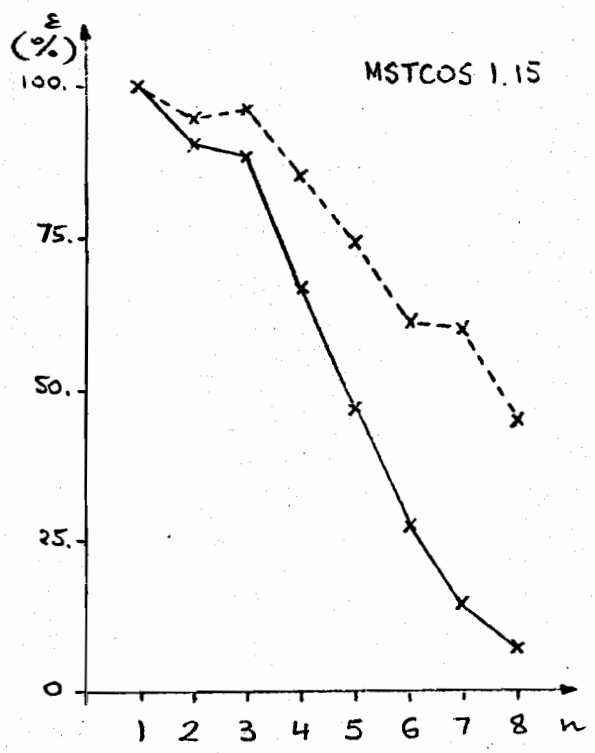

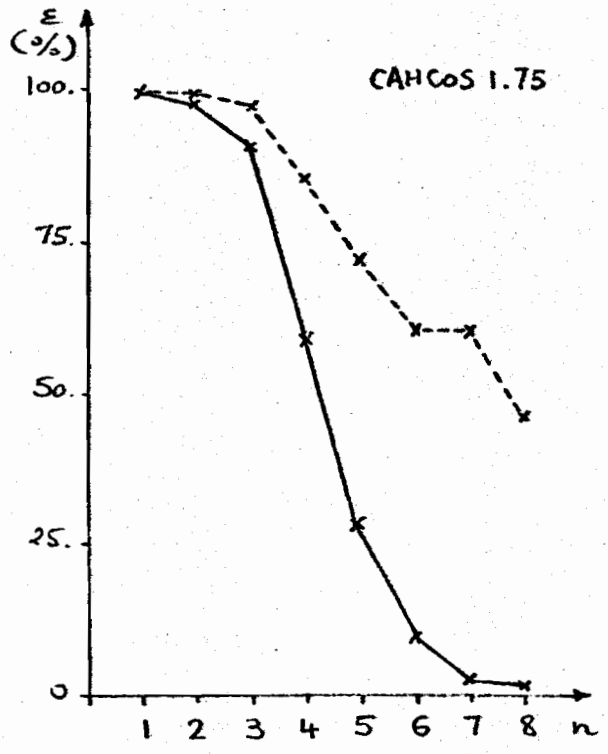

Fig 8 : The ability of the clustering algorithms to find Field's jets.

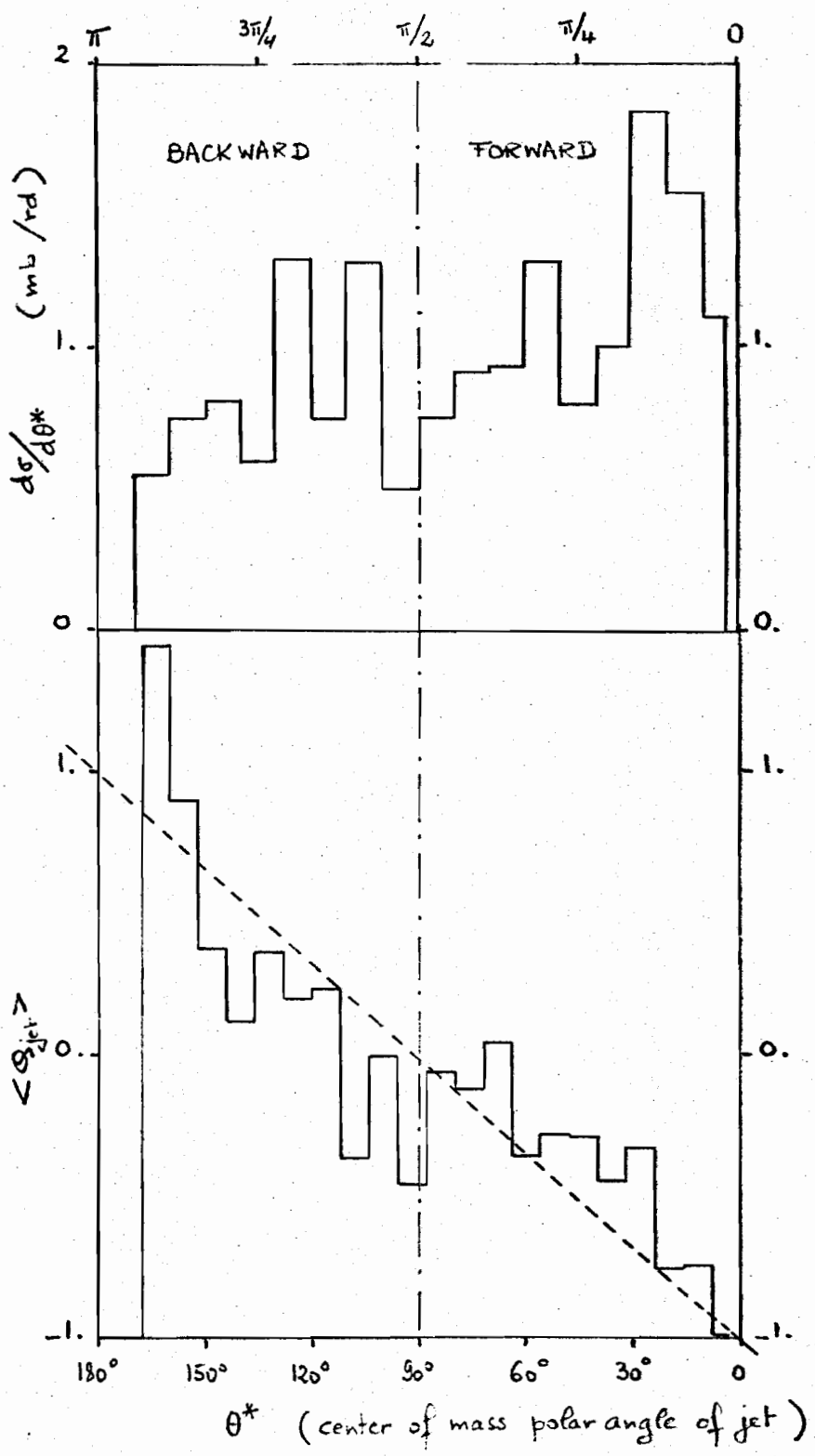
π
3π/4
π/2
π/4
0
BACKWARD
FORWARD
dσ/dθ* (mb/rd)
2
1.
0
1.
0.
1.
0.
-1.
-1.
<θ_jet>
180°
150°
120°
90°
60°
30°
0
θ* (center of mass polar angle of jet)

Fig 9.

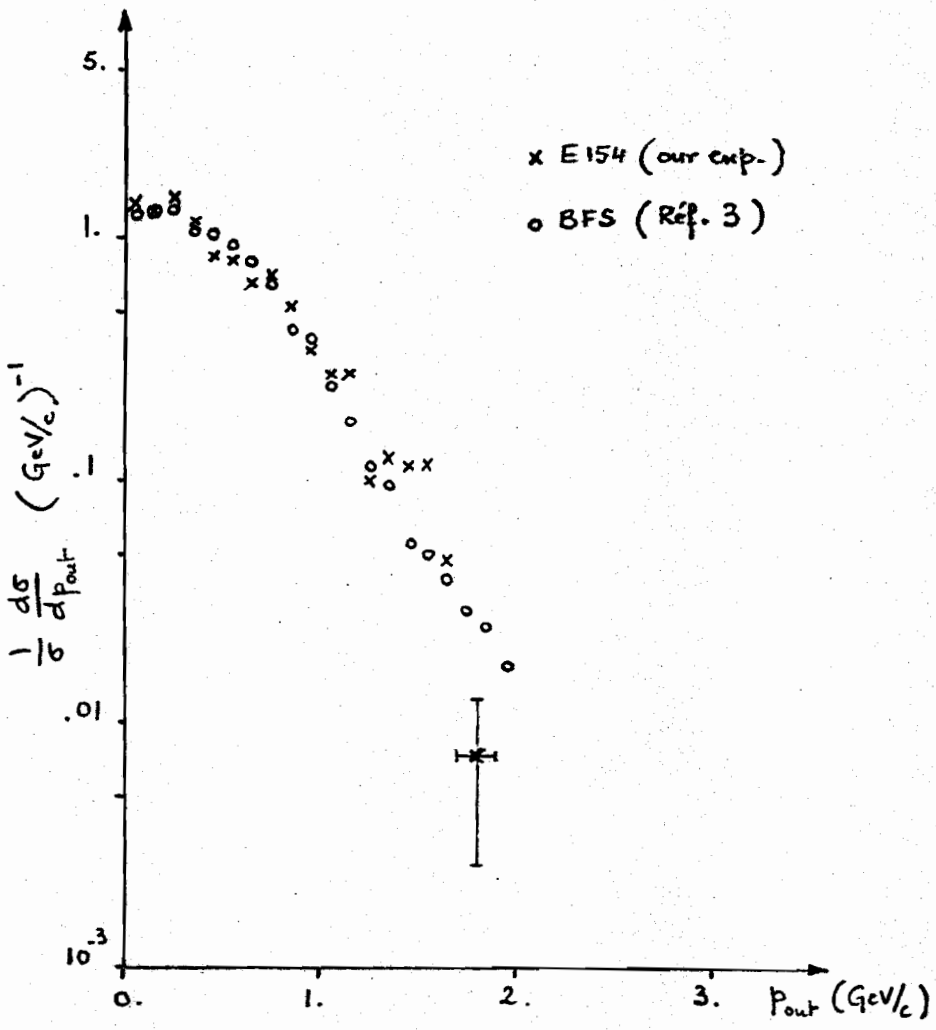

Fig 10 · Distribution of the p_{out} component

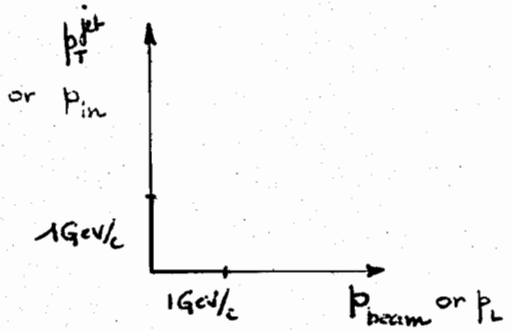

Typical picture of our jet-events

$14 < E_{Tot} < 20$

Balance : $\langle \Sigma p_L \rangle = -.01$ GeV/c

$\langle \Sigma p_{T_{in}} \rangle = +.87$ GeV/c

$\langle p_{out} \rangle = +.56$ GeV/c

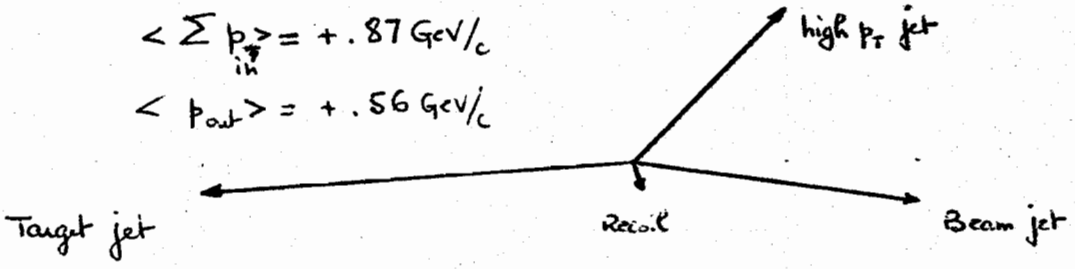

idem for (2 high p_T jets)-events

Balance : $\langle \Sigma p_L \rangle = +.01$ GeV/c

$\langle \Sigma p_{T_{in}} \rangle = +.44$ GeV/c

$\langle p_{out} \rangle = +.77$ GeV/c

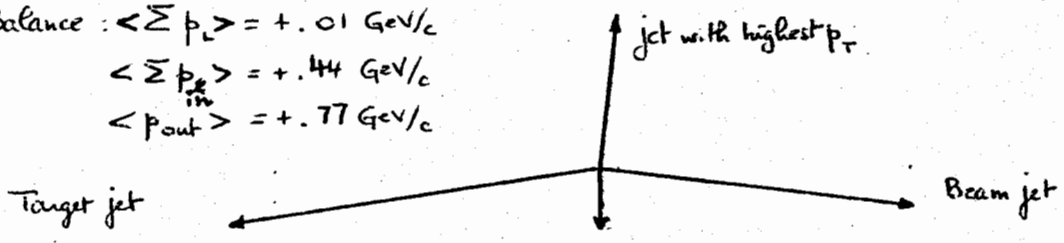

Fig 11 : Momentum balance in jet-events

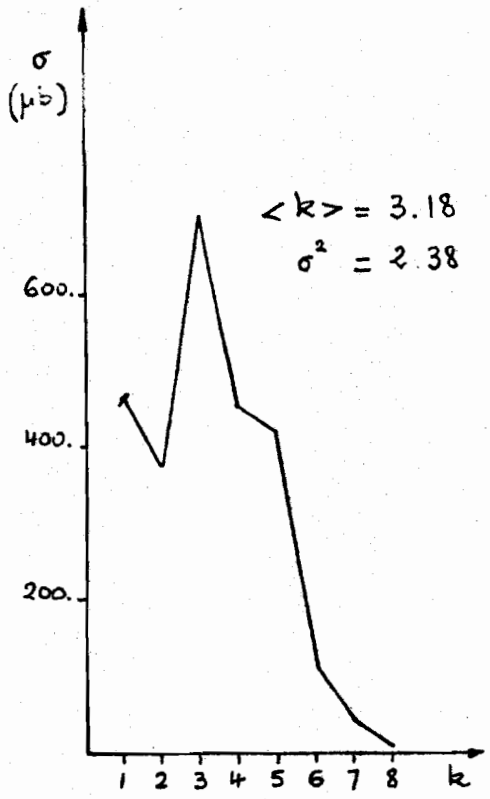

a/ charged multiplicity

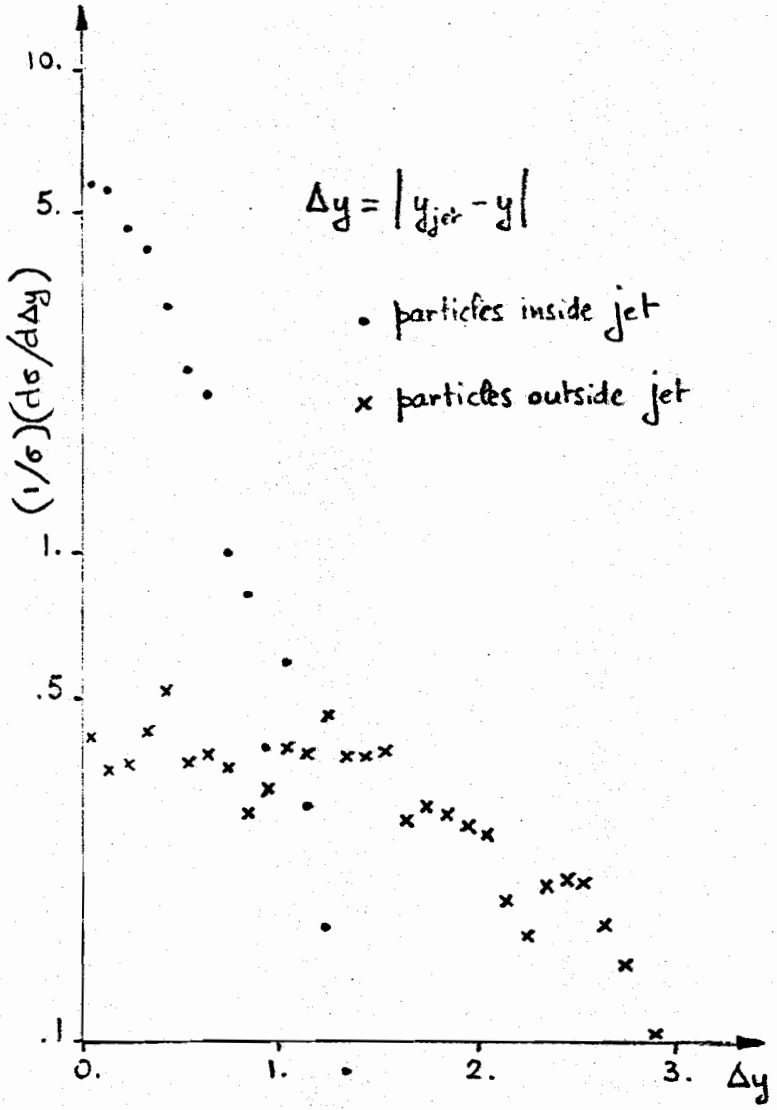

b/ Rapidity correlations

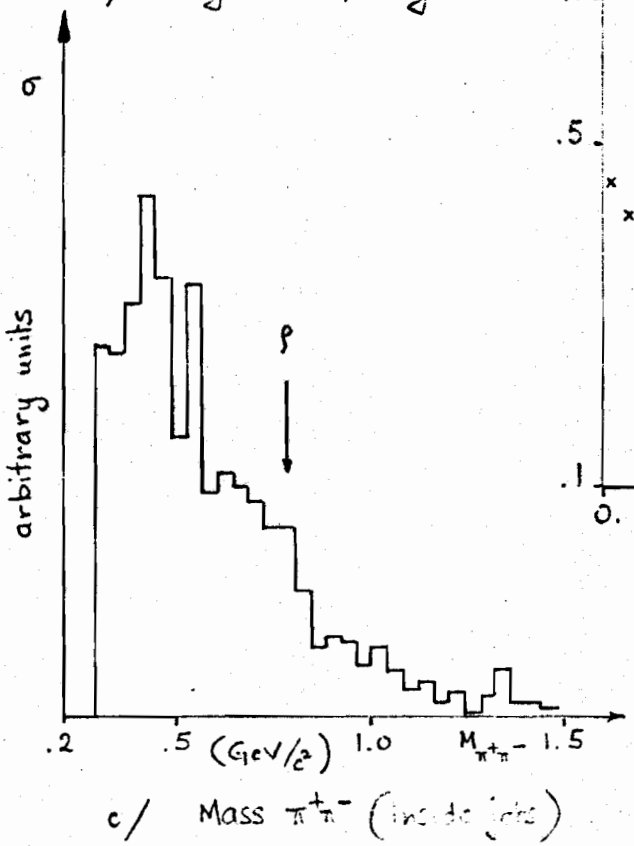

c/ Mass $\pi^+\pi^-$ (inside jets)

Fig 12 Correlations between jet-particles

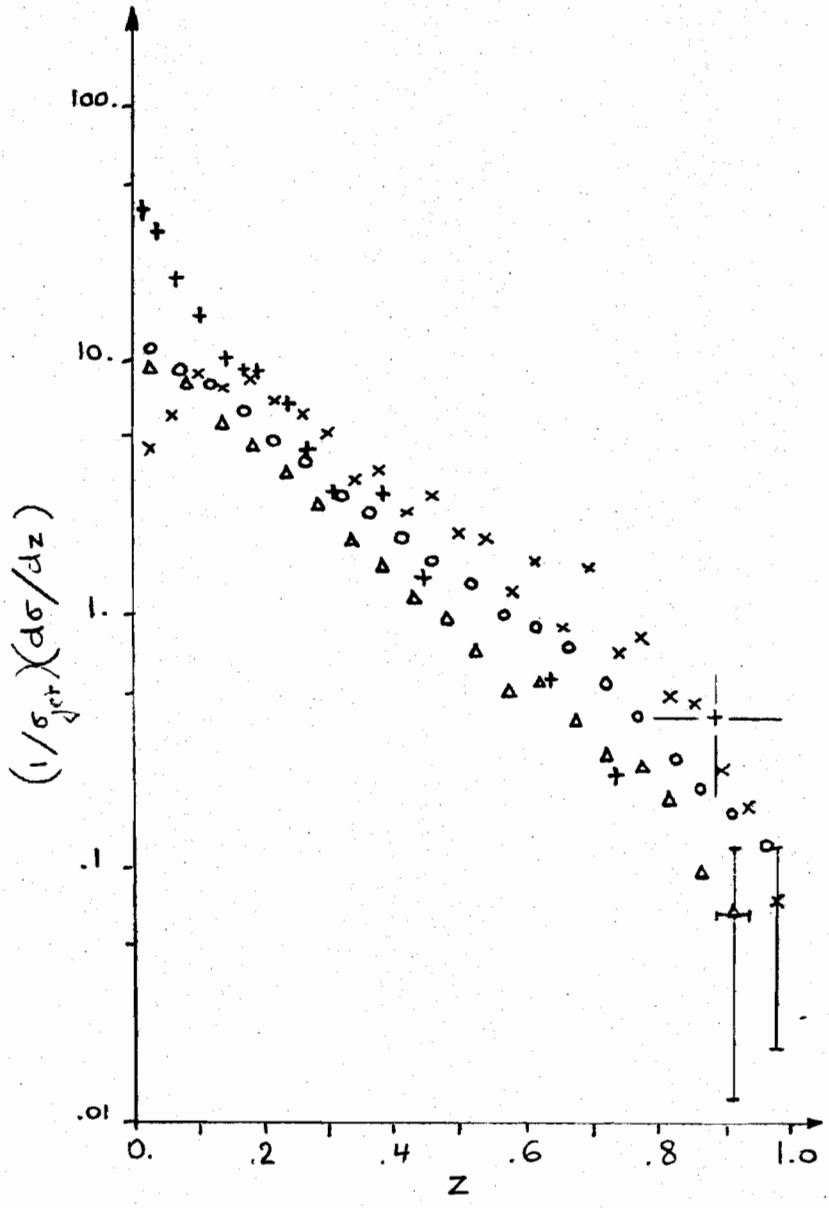

o E260 ; $pp \rightarrow$ jet + X (200 GeV)

▲ $e^+e^- \rightarrow h$

+ $\nu p \rightarrow h + \mu^-$

× this experiment
($p_T > 1.5$; charged only)

Fig 13 · Quark fragmentation

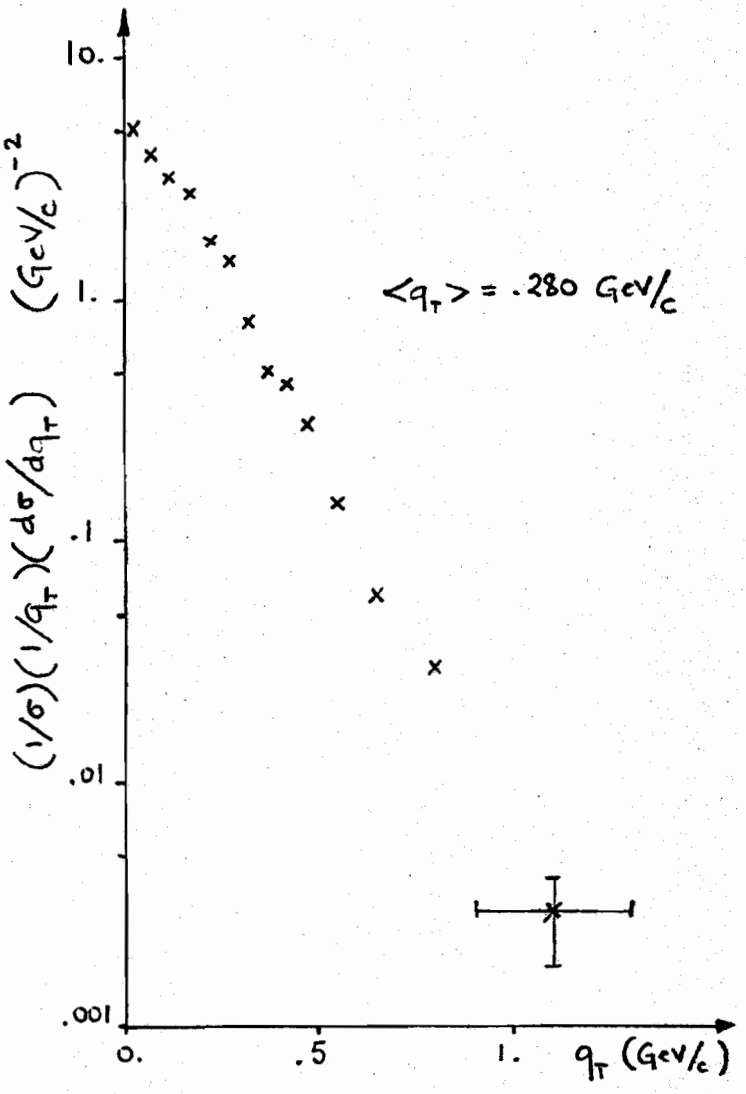
10.
1.
.1
.01
.001
0.
.5
1.
q_T (GeV/c)
$(1/\sigma)(1/q_T)(d\sigma/dq_T)$ $(GeV/c)^{-2}$
$\langle q_T \rangle = .280$ GeV/c

Fig 14.